Published by
NIGERIAN SOCIETY OF PHYSICAL SCIENCES
Available online @ https://journal.nsps.org.ng/index.php/jnsps

J. Nig. Soc. Phys. Sci. 6 (2024) 1730

Journal of the Nigerian Society of Physical Sciences

A DFT study of the optoelectronic properties of B and Be-doped Graphene

L. O. Agbolade[a,b,*], A. K. Y. Dafhalla[c], D. M. I. Zayan[d], T. Adam[a,b,e,*], A. Chik[f], A. A. Adewale[e], S. C. B. Gopinath[a,f,g], U. Hashim[a]

[a]*Institute of Nano Electronic Engineering, Universiti Malaysia Perlis, 01000, Perlis, Kangar Malaysia*
[b]*Faculty of Electronic Engineering and Technology, Universiti Malaysia Perlis, 02600 Arau, Perlis, Kangar Malaysia*
[c]*Department of Computer Engineering, College of Computer Science and engineering, University of Ha'il, KSA*
[d]*Department of computer science, Applied College, University of Najran, KSA*
[e]*Department of Pure and Applied Physics, Ladoke Akintola University of Technology, Ogbomoso, Nigeria*
[f]*Faculty of Chemical Engineering & Technology, Universiti Malaysia Perlis (UniMAP), Taman Muhibah, Jejawi Arau, 02600, Perlis, Kangar Malaysia*
[g]*Micro System Technology, Centre of Excellence (CoE), Universiti Malaysia Perlis (UniMAP), Pauh Campus, 02600 Arau, Perlis, Kangar Malaysia*

Abstract

The electronic and optical properties of Boron (B) and Beryllium (Be)-doped graphene were determined using the ab initio approach based on the generalized gradient approximations within the Full potential linearized Augmented Plane wave formalism (FP-LAPW). Our findings demonstrated that doping at the edges of graphene is notably stable. In both systems, Be- doped graphene proves more efficient in manipulating the band gap of graphene. Both B and Be, induce P-type doping in graphene. B-doped graphene exhibits a negligible magnetic moment of 0.000742, suggesting its suitability for catalytic semiconductor devices. Conversely, Be-doped graphene displays a large magnetic moment of 1.045 μB, indicating its potential in spintronics. Additionally, this study elucidates the influence of the dopant atoms on the optical properties of graphene. These findings underscore a stable and controllable method for modelling graphene at its edges with B and Be atoms, opening new avenues in the design of these devices.

DOI: 10.46481/jnsps.2024.1730

Keywords: Graphene, P-type doping, Dielectrics, DFT, Semiconducting devices

Article History :
Received: 21 August 2023
Received in revised form: 16 September 2023
Accepted for publication: 25 November 2023
Published: 26 December 2023

Communicated by: B. J. Falaye

1. Introduction

Two-dimensional materials such as graphene, hexagonal boron nitride, silicene, and transition metal dichalcogenide have been an active area of research due to their exceptional physical properties for more than two decades [1–3]. The ultra-high electron mobilities and unique optical properties make it an exciting choice for optoelectronic applications [4–6]. However, graphene exhibits a zero-band gap due to its linear dispersion around the Dirac point, which reveals its semi-metallic nature [7–9]. This is responsible for graphene-based logic transistors' poor on/off ratios [10, 11]. Several methods, such as me-

*Corresponding author: Tel.: +2347036508896;
Email addresses: olatomiwaagbolade@gmail.com (L. O. Agbolade), tijjani@unimap.edu.my (T. Adam)

chanical strain, stacking configuration, chemical functionalization, and heteroatom doping, have been employed to engineer a band gap in graphene [12–14]. Among these methods, heteroatom doping is the most promising approach for manipulating graphene's electronic and optical properties [15–17]. This is because it is an efficient approach in modifying its properties towards designing graphene-based devices with specialized functionalities.

Among the different dopant atoms reported in the literature to model graphene for optoelectronics from both computational and experimental approach, nitrogen (N) and B atoms are the natural choice due to their similar atomic sizes to carbon on the periodic table and ease of substitution in graphene [15, 18]. The N and B atoms induces n- and p-type conductivity, respectively [19]. However, N and B atom have shown in different studies to induce a small band gap in graphene, which is responsible for the poor absorption coefficient in N-and B doped graphene for solar cell applications [20]. Recently, Zhou *et al.* [21] investigated the electronic and optical properties of N- and Al-doped graphene, with the N-atom engineering the lowest band gap of 0.21 eV. In another study, Luo *et al.* [22] also reported that nitrogen is the least efficient in tuning the band gap of graphene while investigating the electronic and optical properties of Ti, Fe, and N-graphene. Moreover, Fujimoto *et al.* [23] reported a band gap of 0.32 eV for B-doped systems.

Meanwhile, (Be) which was reported to engineer a wider band gap in graphene has received less attention via the DFT approach [24, 25]. Additionally, most of these studies focused on doping at different lattice positions and percentages, and relatively few studies have addressed doping at the edges of graphene [26, 27]. Therefore, in this study, we modelled an 8-atom graphene supercell decorated with both B and Be singly on the repeating graphene edges.Our calculations revealed that doping of graphene at the edges with both B and Be is not only stable but also preserves the symmetry of the graphene lattice. Notably, Beryllium proved to be more efficient in widening the band gap, making it promising for graphene-based optoelectronics. Furthermore, Section 2 presents the computational details employed in the study of the structural, electronic, and optical properties of graphene using the density functional approach. Section 3 is dedicated to discussion the results of the above-mentioned properties. Lastly, Section 4 concludes the study.

2. Computational Details

The electronic and optical properties of the pure graphene supercell and the doped graphene systems were calculated using the first principles of spin polarization in the full potential linearly augmented plane wave (FP-LAPW) [28] approach as implemented in WIEN2K software [29].The WIEN2k code designed for 3D crystals introduces a suitable, strong vacuum between two identical layers of the surface or 2D crystal to analyze crystal surfaces or a 2D crystal, such as graphene. In these studies, the generalised gradient approximation (GGA) with Perdew Burke Ernzerhof (PBE) was used to calculate the minimum energy [30, 31]. The optimized structural parameters, such as the lattice constant, were determined by the Murnaghan equation of state by fitting the total energy of the structures generated against their volume [32]. The muffin-tin spheres were set at $G_{max} = 12$ for the angular momentum, and the wave functions in the interstitial regions were expanded in a plane wave at $R_{mt}K_{max} = 7$ to reach convergence while determining the properties of the doped graphitic systems. The orbitals for C ($2s^2$, $2p^2$), B ($2s^2$, $2p^1$) and Be ($2s^2$) were considered valence electrons, with a separation energy of -6.0 Ry between the core and the valence electrons [32]. The first Brillouin zone was chosen using the Monkhorst-Pack K point of 1000k for self-consistent field calculations [33]. Additionally, a denser K-mesh of 5000 k was used to successfully capture the first Brillouin zone while computing the density of state. The sampling path of Γ→M→K→Γ was employed to provide the path in the reciprocal space along which the band structures were identified [34]. Given that the system's optical properties depend on the incident electromagnetic waves, the real $\varepsilon_1(\omega)$ and imaginary part $\varepsilon_2(\omega)$ of the dielectric function were used to determine these properties as displayed in equation 1 [35].

$$\varepsilon(\omega) = \varepsilon_1(\omega) + i\varepsilon_2(\omega). \tag{1}$$

Thus, employing the Kramers-Kronig relation in equation (2), ε_2 in the long wavelength limit can be determined using the following expression [36, 37]:

$$\varepsilon_2(\omega) = \frac{2e^2\pi}{V\varepsilon_0} \sum_{v,C,K} \left| \left\langle \psi_K^C \right| \hat{u} \cdot \hat{r} \left| \psi_K^V \right\rangle \right|^2 \delta\left((E_K^C - E_K^v) + (-\omega)\right), \tag{2}$$

where, ω, ε_0, *and* V represent the angular frequency, permittivity of free space, and volume of the supercell of the electromagnetic radiation, respectively. The valence and conduction bands are denoted by c and v. Thus, $\hat{u}$ *and* $\hat{r}$ represent the incident electromagnetic field's polarization vector and position vector, respectively [34, 38].

$$\varepsilon_1(\omega) = 1 + \frac{2}{\pi} A_{coeff} \int_0^\infty \frac{dw\, \varepsilon_2(w')}{w'^2 - w^2} dw'. \tag{3}$$

The dielectric function as denoted above by $\varepsilon(\omega)$ and other parameters of other optical properties such as absorption coefficient (A_{coeff}), optical refractive index n (ω), energy loss function L (ω), extinction coefficient K (ω) and optical conductivity σ (ω) are denoted by these symbols in equation eqs. (4) to (8) respectively [39].

$$A_{coeff}(\omega) = \frac{(\sqrt{2w})}{(\sqrt{v})^{1/2}} \left[\sqrt{\varepsilon_2^2(\omega) + \varepsilon_1^2(\omega)} - \varepsilon_1(\omega) \right]^{\frac{1}{2}} \tag{4}$$

where v represents the velocity of light.

The modulation of the refractive index is employed to determine energy against wavelengths. The refractive index of Be/B-doped graphene were determined using equation (6) and (7).

$$n(\omega) = \varepsilon_1\left(\sqrt{\omega}\right) + \left(\frac{\sqrt{\varepsilon_{1(\omega)} + \varepsilon_2(\omega)^2}}{2} \right). \tag{5}$$

$$k(\omega) = \left(\frac{\sqrt{\varepsilon_{1\,(\omega)} + \varepsilon_2\,(\omega)^2}}{2} \right) - \varepsilon_1 \left(\sqrt{\omega} \right), \tag{6}$$

where n (ω) and k (ω) in equation (6) and (7) represent the real and the imaginary part of the complex refractive index with the relation, $\check{\upsilon} = \eta(\omega) + ik(\omega)$.

$$L\ (\omega) = \left(\frac{\varepsilon_2}{\varepsilon_2(\omega)^2 + \varepsilon_1(\omega)^2} \right). \tag{7}$$

The electron energy loss function determines the collective excitation of a particular system and is obtained using equation (8). The optical conductivity can be calculated using:

$$\sigma\ (\omega) = -\, i \frac{\omega}{\sqrt{16\pi^2}}\ \lfloor \varepsilon(\omega) - 1 \rfloor . \tag{8}$$

3. Results and discussion

3.1. Structural Properties

The pristine graphene considered has a space group symmetry of 194 $P6_3/mmc$ and the value of the lattice parameter was set to be $a = b = 2.46$Å and c = 10 Å. These values are consistent with other theoretical and empirical values [34, 40, 41]. The unit cell of graphene consists of two carbon atoms, which is contained in a rhombus with the hexagonal lattice in real space rotated by 90^0 to create an equivalent reciprocal lattice [42]. The positions chosen are at a (0, 0, 3/4; 0, 0, 1/4) and a (1/3, 2/3, 3/4; 2/3, 1/3, 1/4). The supercell of pristine graphene with the dimension 2x2x1, comprised of 8 Carbon atoms was constructed as displayed in Figure 1a.

Subsequently, B and Be, atom were chemically substituted in the supercell structure of graphene at the edges separately which maintained the hexagonal structure of graphene. The crystal structure of the optimized pristine graphene supercell and B and Be-doped graphene was illustrated in Figure 1 [43]. The minimum energy and volume of the optimized pure graphene was determined by executing volume optimization programme on WIEN2K. The diagram reveals that when Murnaghan Equation of state is employed, the minimum energy of the system (i.e., -304.832 Ryd) is determined for the cell volume V_o =355.97384 bohr^3. The value of the optimized lattice parameter obtained for pure graphene emerges as a = b = 4.663 au, equivalent to 2.468Å, the vacuum emerges as, c = 18.897 approximately 10.00 Å with a C – C bond length equal to 1.42Å.

To determine the impact of B and Be dopants on the arrangement of the pristine graphene supercell mentioned earlier, one carbon atom was substituted at the edges of graphene with B and Be atoms singly to generate B-doped and Be-doped graphene. This results in a 12.5 % of B and Be in graphene. We observed that the hexagonal lattice of graphene remained undistorted after substituting these elements at the edges with the same sublattice sites, despite the differences in their core and the outermost electron configurations compared to graphene. This is consistent with other findings reported in literature [34, 44]. However, the in-plane substitution of either of B or Be in any two carbon atoms may result in the breaking of the hexagonal 2D lattice of graphene due to the size of the molecular radius of Be and B relative to carbon.

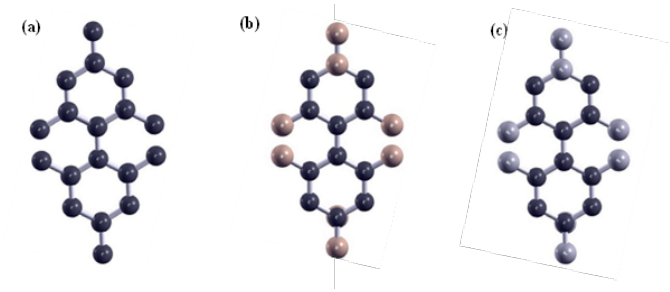

Figure 1. The supercell structure of (a) Pure (b) B and (c) Be-doped graphene.

The relaxation of the lattice parameter was carried out to obtain the minimum energy, and this is revealed in Figure 1b and Figure 1c for B and Be-doped graphene supercell. As reported earlier, hexagonal lattice structure and symmetry of graphene chosen was maintained with 194 $P6_3/mmc$ as the space group for the most relaxed structures for the doped systems. The supercell's parameters for B- and Be-doped graphene were determined and observed to be a = b=4.968Å and c = 10.066Å with $\alpha = \beta = 90^0$, $\gamma = 120$. We observed that the bond length of both B-C and Be-C is 1.415 Å which is a slight distortion compared to the C-C bond length of 1.42 Å, due to their position in the lattice of graphene which was also reported by Zeng at al. [45]. The minimum energy of the B-doped graphene system (i.e., -1166.071 Ryd) is determined for volume, V_0=1452.3733 bohr^3 while for Be-doped graphene the minimum energy (i.e., -1124.9432 Ryd) calculated for the cell volume V_0=1452.3733 bohr^3.

3.2. Electronic Properties

In this section, the electronic properties of optimized pristine graphene, as well as graphene geometry doped with (B), and (Be). We examined the influence of these dopants on graphene's electronic band structure. It was observed that the orbitals associated with C, B, and Be dopants are responsible for the band gap in graphene. Figure 2 reveals the electronic band structure of the optimized pure and doped graphene systems investigated. Moreover, as shown in Figure 2a, the convergence of the maximum valence and minimum conduction band at the K point results in a zero-band gap, indicating its semi-metallic behaviour. The relationship between these two bands determines the appearance of high electrical conductivity with high electron mobility from the unoccupied band to the occupied band. As a result, graphene behaves like a semi-metal with a zero-band gap, as the two P_z bands meet at the Fermi level's K-point, and this is consistent with previous findings established in the literature, validating the accuracy of our results [40, 46, 47].Therefore, the chemical substitution of B and Be alters the charge carrier concentration of the material.

Figure 2b vividly illustrates the effect of B on the band structure of graphene, with an increased number of bands due to the optimized B-doped graphene. However, B is less elec-

tronegative than carbon and undergoes sp^2 hybridization because they both have similar sizes due to their position on the periodic table. As a result of B's electron-deficient character causing p-type doping, the Fermi level seen in Figure 2b is 2.2 eV below the Dirac cone in the unoccupied band. The substitution of B in the graphene structure causes a distortion in the symmetry of the C – C atoms, creating a band gap of 0.4 eV around the Dirac cone. This observed change indicates a decrease in the conductivity of graphene. This is consistent with previous studies [41, 48, 49].

In Figure 2c, the influence of the Be atom substitution in graphene is observed. Our calculations show that, like the B-doped graphene, the Fermi level, as observed in Figure 2c has shifted 2.6 eV below the Dirac cone in the unoccupied band, resulting to p-type doping. However, a wider direct band gap of 0.9 eV was induced, showing that Be is more efficient than B at widening graphene's band gap. The introduction of Be in graphene resulted in increased stability and reduced conductivity compared to pure and B-doped graphene, as evidenced by band lines crossing the conduction band. Our calculated energy band gap for one atom substituted into eight atoms of the Be-doped system is close to the energy gap obtained by Ullah *et al.* [50] when four carbon atoms replaced four Be atoms at 12.5%, demonstrating the accuracy of our results [51]. The total and partial densities of state for pure graphene were compared to those of B- and Be-doped graphene in Figures 3, 4, and 5. The density of state (DOS) gives vital details about the transition of electrons from the valence band to the conduction band and predicts the occupancy of electronic orbitals during an interval of energy changes due to the presence of dopant atoms, which affects the performance of the device [32]. The density of states at the Fermi level is crucial for a material's electronic and electrical conductivities.

The calculated total density of state (TDOS) of pure graphene in Figure 3 reveals that pure graphene metal has a vanishing density of state at the Fermi energy, typified by linear dispersion around this point, as indicated by the band structure in Figure 3a. In Figure 3a and b, a sharp peak in the conduction band appears for both TDOS and TDOS_PDOS at 8.85 eV for pristine graphene. We observed three sharp peaks each in the conduction band in Figure 3a-b at 2.5 eV, 12 eV, and 16 eV, while 13.8 eV is an extended peak. Two peaks appear in the valence region for both figures, with an extended peak at -7.5 eV and a sharp peak at -2. 5 eV. As seen in Figure 3c, the C-p-orbital of the C atom has the highest contribution, with the C-s-states of carbon contributing less. Moreover, a prominently distinct peak at about 8.85 eV in the conduction band and in the valence band is primarily attributed to the presence of the C-p states, consistent with findings reported by several studies [52–54].

As shown in Figure 4, the point relevant to zero density of state at E_F relative to the Dirac cone in pure graphene appears at +2.20 eV for B-doped graphene, with the Fermi level moving to the valence band, implying that this system is a p-type material. The linear dispersion observed at the Fermi level of pure graphene vanishes due to the impact of B, and an overlapping emerges in the valence and conduction bands at the Fermi level, indicating a reduction in the conductivity of graphene. Therefore, no energy levels are seen in this range of energy based on the energy gap found in the density of the state spectrum.

Furthermore, the peaks at 0.00 and 2.20 eV, both with a value of 3.56 eV, contribute significantly to the material's electronic properties due to their proximity to the Femi level, as shown in Figure 4b. The intensities of the peaks for the total density of state of B-G appear at the valence band, which appears at 0.0, 2.0, 4.6, 5.0, and 7.5, respectively, while in thee CB the intensities peaks are at 12.0, 13.8, 17.8, respectively, as displayed in Figure 4a. These values are significantly higher than the values obtained for pure graphene. Therefore, by calculating the partial density of states on different atomic sites, as revealed in Figure 4c, the band gap caused by B doping was determined.

Furthermore, in Be-doped graphene, the change in the Fermi level is 2.26 eV, with a wider gap as observed in the band structure of (Be), which reveals that it is more effective than B in opening an energy gap in graphene. As illustrated in Figure 5a-b, the Fermi level shifted to the valence band, with the system also indicating a p-type material, which is consistent with different studies [55–57]. The chemical substitution of Be into the lattice of graphene has led to a much-reduced conductivity when compared with both pure and B-doped graphene, which appears in the band structure. There is an overlap of both bands at the Fermi level, with a DOS value of 6.2 eV as presented in Figure 5a. The Be-doped graphene also reveals that at the Fermi level, the linear dispersion disappears Figure 5a-c.

Additionally, the peaks at 0.00 and 2.26 eV, both with a DOS value of 6.2 and 3.8 eV, greatly affect the material's electronic properties because of their proximity to Fermi levels, as shown in Figure 5a-b. The peak values of the TDOS in the valence band were determined to be 2.7, 3.5, 3.1, 8.0, 4.8, and 2.9 , corresponding to energies of -1, -2, -3, -4, -5, and -8 eV, respectively. In the conduction band, the DOS values vary at 3.8, 4.0, 7.6, 5.2, 5.2, corresponding to energies of 3.8, 10, 11.5, 14 and 18 eV, respectively. Furthermore, Figure 5b reveals the partial density of state plot, illustrating that the P orbital of both C and Be is the major contributor to the bonding despite Be having an electronic configuration of $1S^2 2S^2$. However, due to the small gap between the two orbitals, the electron in the 2s orbitals is partially promoted to the 2p orbitals, resulting in covalent bonding.

3.2.1. Magnetic Moment

The calculated magnetic moments for pure, B, and Be-doped graphene are presented in Table 1 based on the inputs of each atomic element in the system configurations, with each atom's interstitial as well as the spin moment highlighted. The negligibility of the values of the magnetic moment of the composition of all the atoms in pure and B-doped graphene verifies the nature of the total and partial densities of the state curve and their non-magnetic character for both systems. The planar structure of the B-G was retained. The B atom is a P-block element with an electronic configuration of $1s^2 2s^2 2p^1$. The B atom, when substituted into graphene, undergoes sp2 hybridization, and no unpaired electrons or breaking of the sym-

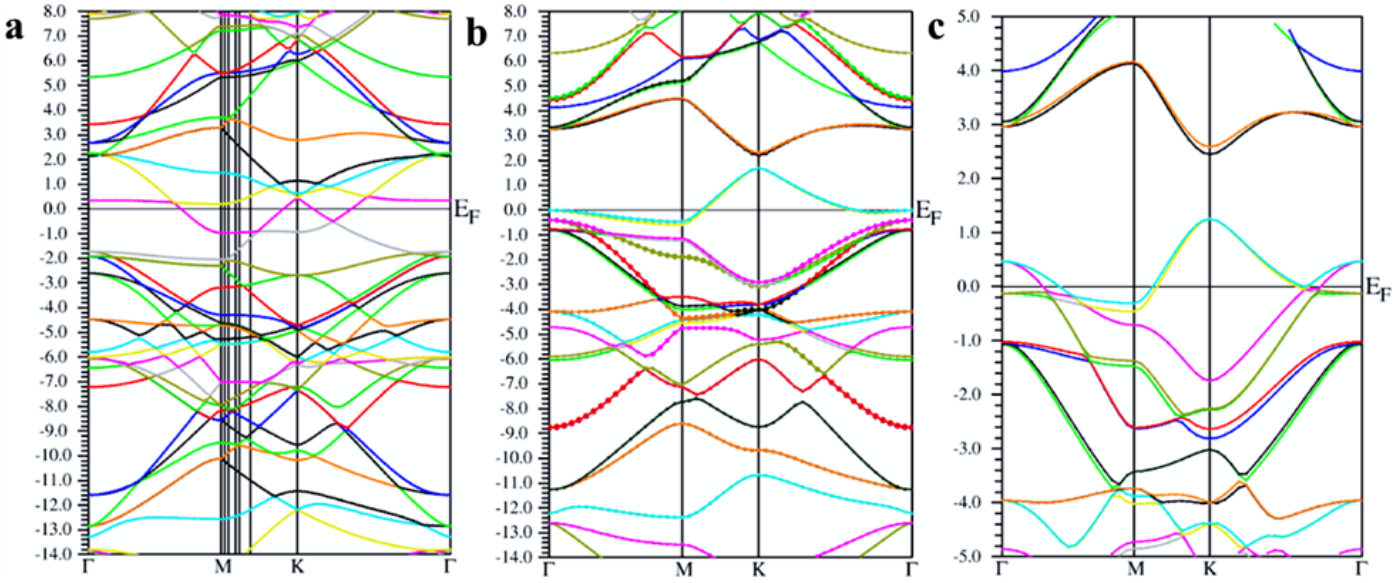

Figure 2. The calculated band structure of (a) Pure (b) B- and (c) Be-doped graphene.

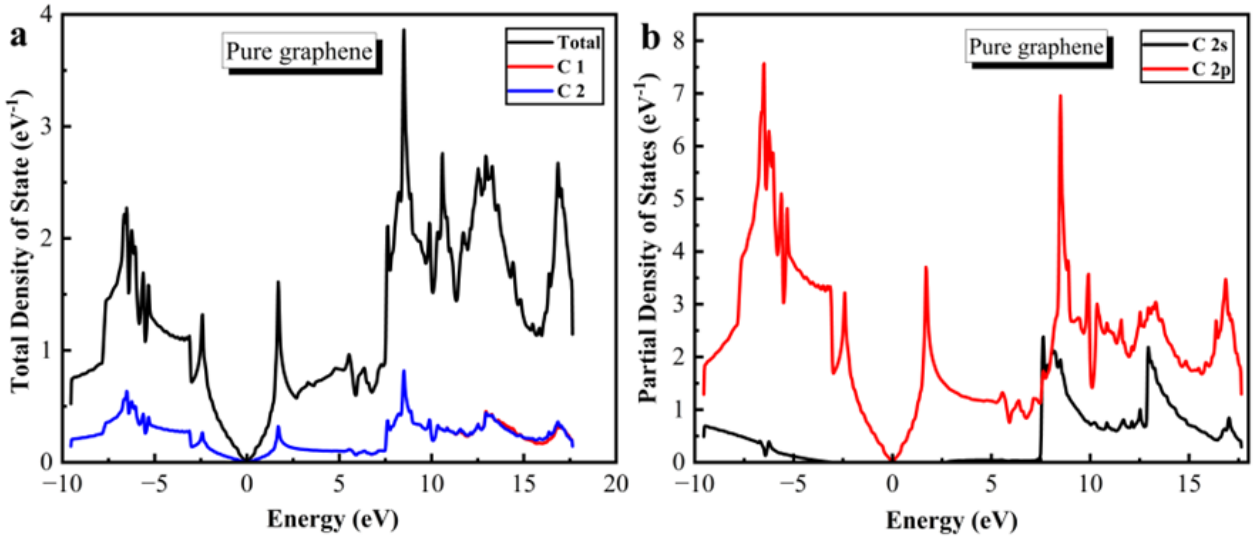

Figure 3. The calculated (a) total density of state (b) partial density of state of pure graphene.

metry occurred. The distribution of the dopant atoms within the graphene sheet has a significant impact on how the dipole moment of B-G behaves. However, in this case, there is no magnetism in the system. These reports are reported in different studies and show that B-doped graphene can be adopted in catalytic and semiconductor applications [58–60]. Furthermore, due to Be's electronic configuration, Be-G is limited to sp hybridization, $1s^2 2s^2$. A total magnetic moment of magnitude 1.045 μ_B was obtained due to the paired electrons and a small distortion in the symmetry of graphene. Urias reported a total local magnetic moment of 0.29 μ_B.

The difference in the value of the magnetic moment can be attributed to the difference in the size of the systems and dopants considered [6]. However, in an earlier study, He *et al.* [61] reported a magnetic moment as large as 1μ_B agreeing with our result. Therefore, our results show that Be atoms are more reactive and have a more significant impact than B atoms by inducing a magnetic moment in graphene. This is also evidenced by the density of the state's plot and several other findings [62–64]. The calculated magnetic moment (μ_B) for Pristine and B and Be doped graphene is presented in Table 1 .

3.3. *Optical Properties*

The influence of the B and Be atoms on the optical properties of graphene will be discussed in this part, with an obvious change observed in graphene's electronic properties by chemically substituting these atoms in graphene's hexagonal structure.

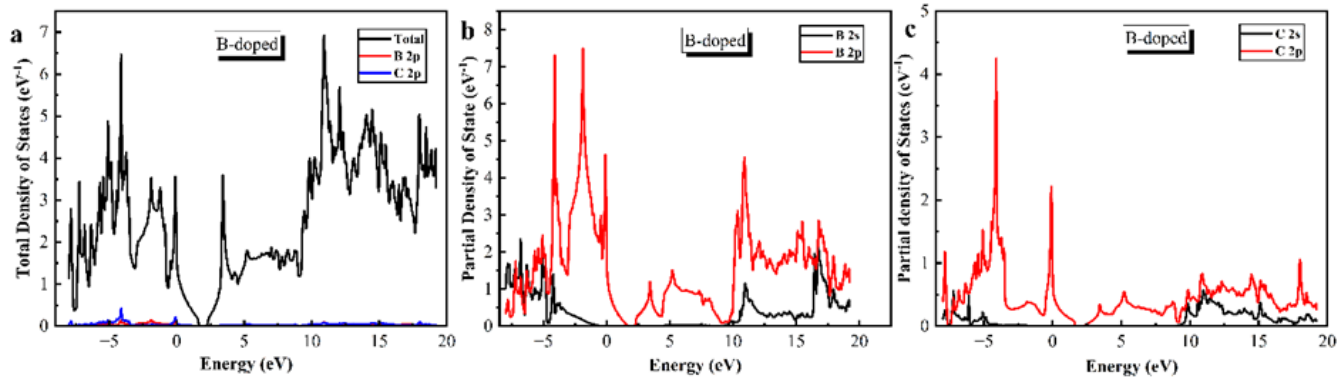

Figure 4. The calculated (a) Total density (b) Total and Partial density of State (c) Partial density of state of Be-graphene.

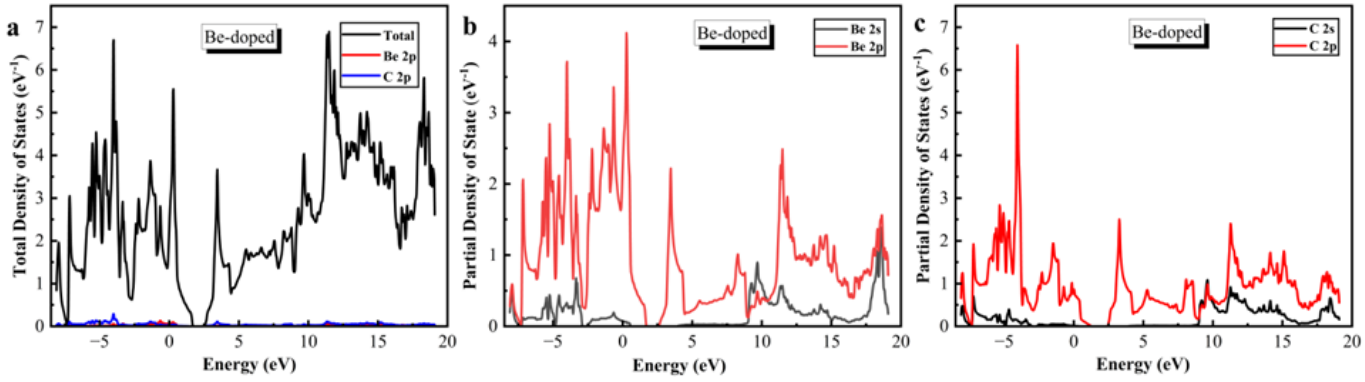

Figure 5. The calculated (a) Total density of state (b) partial density of states showing the atomic orbitals of Be (c) partial density of states showing the atomic orbitals of C for Be-G.

Table 1. The calculated magnetic moment (μ_B) for Pristine and B-/Be doped Graphene Sample.

	Pure	B-doped	Be-doped
Magnetic Moment in interstitial	−0.00307	− 0.00456	0.64356
Magnetic Moment in Sphere 1	−0.00319	0.00000	− 0.01026
Magnetic Moment in Sphere 2	−0.08775	− 0.00012	− 0.01320
Magnetic Moment in Sphere 3	NA	− 0.000417	0.08582
Magnetic Moment in Sphere 4	NA	−0.00028	0.04432
. Spin Magnetic Moment in a Cell	−0.07522	−0.00742	1.04599

3.3.1. Dielectric Properties

The main optical properties of the material are determined by the dielectric function, which also depicts the structure of the solid energy band and a variety of spectrum information [108]. The real $\varepsilon_1(\omega)$ and imaginary part $\varepsilon_2(\omega)$ of the dielectric function of pure graphene is shown in Fig 6a-b as a function of frequency in the parallel, $E_{\parallel}$ and perpendicular, $E_{\perp}$ polarization of the electromagnetic (EM) waves in the energy range of 0-14 eV. Graphene's absorption spectra are related to the imaginary part of the dielectric function.

In this part, Figure 6b shows two distinct peaks at 4 eV in the ultraviolet range, with a sharp fall at the visible light range at 8 eV, and a maximum of 13.8 eV at the infrared range in the parallel polarization of the electromagnetic wave. The locations of these two peaks are consistent with the findings reported by Olaniyan *et al.* [38], [109] and Sedelnikova *et al.* [67]. The origin of the peak at 4 eV can be attributed to the transition between the electronic states of graphene from the higher valence band to the lower conduction band ($\pi \rightarrow \pi*$) in the M-K direction in the region of M in the Γ-M path, as illustrated in Figure 2, while the strong resonance observed at 13.8 eV results from the changes from the lower conduction band to the higher valence band, which generates its strongest peak at the higher energy range ($\sigma \rightarrow \sigma*$) in both the X-M and M-K directions at the M point [67, 68]. Moreover, in the perpendicular polarization, a peak emerges at 11 eV and falls at 13.8 eV, caused by the ($\pi \longrightarrow \sigma^*$)and ($\sigma \longrightarrow \pi^*$) inter-band changes between the material. In equation (1), the Kramer-kroing rela-

tion is used to determine the real part of the dielectric function $\varepsilon_1(\omega)$ with the calculated static constant for both parallel and perpendicular polarization found at 33.5 and 2.00. The $\varepsilon_1(\omega)$ at the parallel polarization has a peak at 4.2 eV in the ultraviolet range, which spreads across the visible range till it reaches a maximum of 13.6 eV in the infrared range while the perpendicular polarization in the EM waves reaches a peak at 10.5eV in the far red region [69, 70].

Therefore, we have calculated how the modeling of graphene with different atomic elements (Band Be) affects the height and position of the imaginary and real parts of the dielectric function in doped graphene systems. Figure 6c-d depicts the imaginary and real parts of the dielectric function to show how B-G differs from pristine graphene. The well-defined peaks observed in pristine graphene appear to have redshifted, i.e., they change to a broader plateau on the axis with the frequency spread across the energy range of B-G and the parallel polarization vanishes at this range, based on the results for $E_\perp$ polarization in Figure 7b.

The calculated static dielectric constant for B-doped system in both $E_\parallel$ and $E_\perp$ polarization is less than zero, as illustrated in Fig 7a. The same observation is made with Be-G in the EM spectra at the $E_\parallel$ and $E_\perp$ polarization. The discussion that follows focuses on the other optical properties of graphene, like the absorption, energy loss function, reflection, and refractive index of a pure and doped system, all of which are deduced from the dielectric function.

3.3.2. *The Absorption Spectra of the systems*

The absorption coefficient determines how much light is absorbed in optical materials per unit length [32]. It is the process by which an EM wave travels through a material and absorbs energy, resulting in electron excitation. As illustrated in Equation 4, the absorption coefficient is derived from the dielectric function. Figure 7a depicts the pure graphene absorption spectrum in both $E_\parallel$ and $E_\perp$ polarization along the electromagnetic spectra.

In Figure 7a, we observed that pristine graphene has two prominent peaks in the spectrum at optical frequencies of 4.2 and 13.6 eV in the $E_\parallel$ electromagnetic polarization. The intensity of the second peak at 13.6 eV is higher than the first peak. However, the first peak has a wider frequency spreading across the ultraviolet and visible region, which coincides with the imaginary dielectric function energy in the parallel polarization for pure graphene. These results are consistent with several theoretical studies [34, 67, 71].

However, the obtained peak at 4.2 eV is underestimated compared to the reported empirical value due to the GGA-PBE functional employed in our calculations. The pristine graphene has the highest light penetration and absorption coefficient in the parallel electromagnetic polarization compared to the other systems considered in this study. Furthermore, in the $E_\perp$ polarization pristine graphene has an extended peak at 12 eV and at an interval of 9.8 eV − 12.6 eV, it is higher than the $E_\parallel$ in this range. However, the results obtained show that the optical property of pristine graphene depends on the parallel polarization of the EM wave based on its stronger light penetration and high absorption coefficient.

The effect of B and Be atoms on the absorption coefficient of graphene as it affects the positions and intensities of the major peaks in relation to the $E_\parallel$ and $E_\perp$ polarization is discussed further . The absorption spectra of the B-doped system illustrated in Figure 8b show a decrease in the absorption peak observed in the $E_\parallel$ polarization of pristine graphene with different spikes which spread across the visible region with a broader frequency and blue shifted relative to the position of the $E_\parallel$ polarization of pure graphene.

However, for the $E_\perp$ polarization in B-doped systems, the two peaks observed at 10.6 and 12.6 eV are well-defined compared to pristine graphene and it also blue shifted towards the $E_\perp$ polarization of pristine graphene. However, the B-doped system in $E_\perp$ polarization of the has a stronger light penetration compared to pristine graphene at higher energy in the infrared region with well-defined peaks and wider frequency. While in the visible range, the $E_\parallel$ polarization of B-G still has higher absorption coefficient than in the $E_\perp$ electromagnetic polarization. However, the intensity of the absorption coefficient of B is much reduced compared to pure graphene.

For the Be-doped system, the peak observed at 4 eV in pristine graphene has fallen further with more spikes relative to both pure and B-G. However, the frequency of the peaks is more spread across the energy range when compared to B-G. The parallel polarization of the electromagnetic wave is characterized by two prominent peaks, as illustrated in Figure 7c, at 10.5 eV and a well-defined peak at 12.3 eV. Moreover, the Be-doped system shows stronger light penetration and a more pronounced absorption coefficient in the $E_\perp$ polarization in the infrared range at the interval 9.6 eV − 12 eV when compared to pure and B-G. Thus, graphene has the least light absorption in the $E_\perp$ polarization and the highest absorption in the $E_\parallel$ polarization as illustrated in Figure 7.

3.3.3. *Complex Refractive Index and Reflectivity of the Systems*

The refractive index n (ω) and the extinction coefficient k (ω), which are the real and imaginary refractive index, respectively determined as normal incidence as represented by the equation below, are combined to form the complex refractive index $\tilde{n}$ (ω) [32, 72].

$$\widetilde{n}(\omega) = n(\omega) + \ +ik(\omega) \tag{9}$$

The refractive index determines the potential of a material to permit the passage of EM waves, while the extinction coefficient reveals the behaviour of the material because of the attenuation of the EM waves at a given wavelength [32]. Figure 8a shows the normal refractive index spectra of pure graphene in the $E_\parallel$ and $E_\perp$ polarization as a function of energy. The static refractive index n (ω) for pristine graphene is 5.9 for the $E_\parallel$ and 1.2 for the $E_\perp$ polarization. The $E_\parallel$ polarization of the electromagnetic wave has two peaks, with the highest peak value of the n (ω) for pure graphene appearing at 2.4 with an optical frequency of 3.8 eV, while the second peak appears at 1.8 at the optical frequency of 11.2 eV.

However, a peak at 2.2 appears in the $E_\perp$ polarization of light at the optical frequency of 10.3eV, as illustrated in Fig-

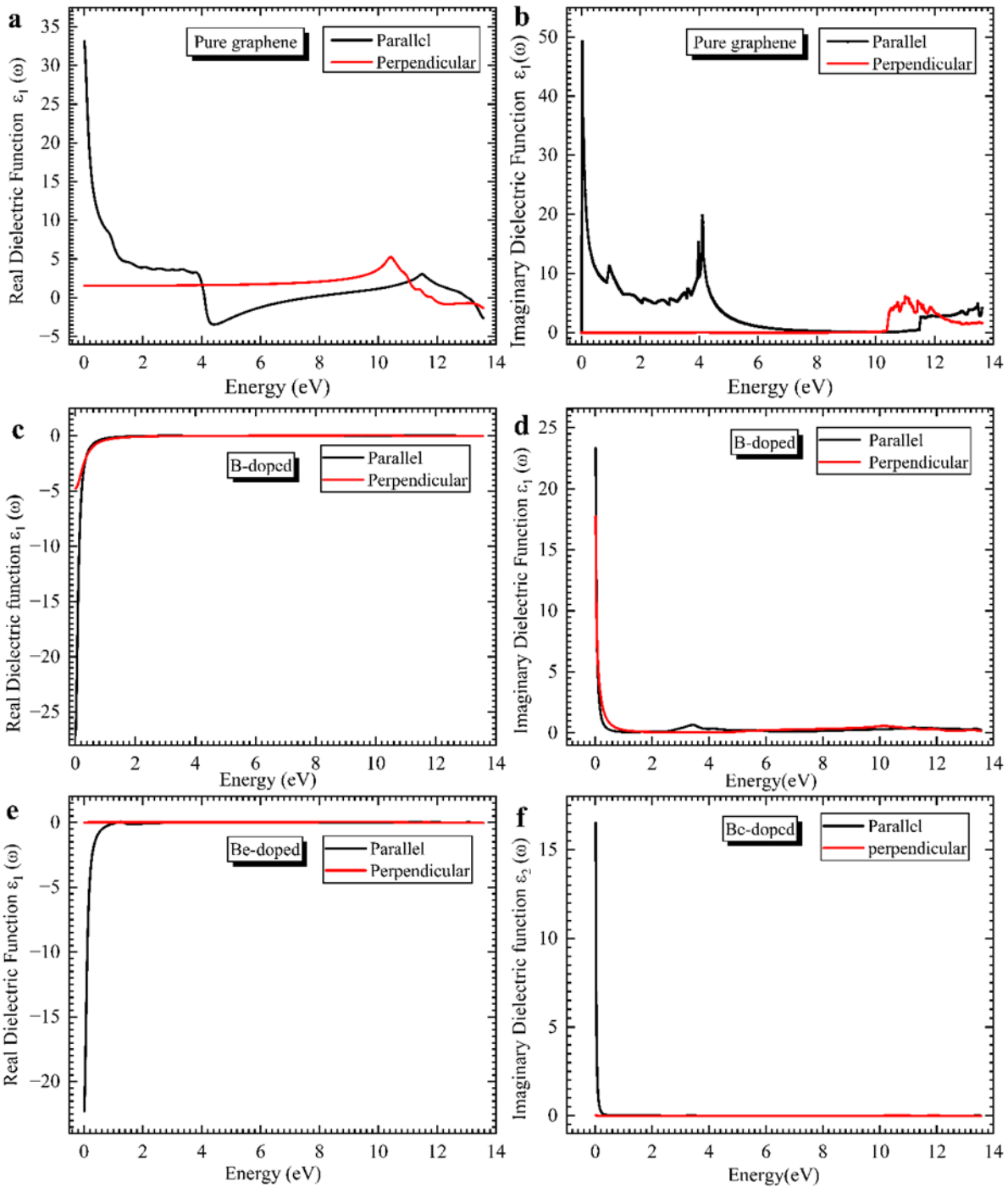

Figure 6. The calculated (a) real part $\varepsilon_1(\omega)$of the dielectric function (b) imaginary part ε_2 (ω) of the dielectric function of pure graphene (c) real part ε_1 (ω) of the dielectric function (d) Imaginary part ε_2 (ω) of the dielectric of B-G (e) real part ε_1 (ω) of the dielectric function (f) Imaginary part ε_2 (ω) of the dielectric of Be-G.

ure 8a. The peaks found in the spectra are a great sign of the refractive index's highest value at the optical frequency [34]. However, as illustrated in Figure 8b-c, the intensity and positions of the peaks observed in pure graphene change drastically and drop to a negligible value in, $E_{\|}$ and $E_{\perp}$ polarization of EM wave for both B and Be doped systems, which corresponds to the results obtained for the real dielectric function in both, $E_{\|}$ and $E_{\perp}$ polarization of light with the static n (ω) of B reaching a maximum at 71 and 93 for the, $E_{\|}$ and $E_{\perp}$ polarizations, respectively. The Be-doped system's static refractive index appears at

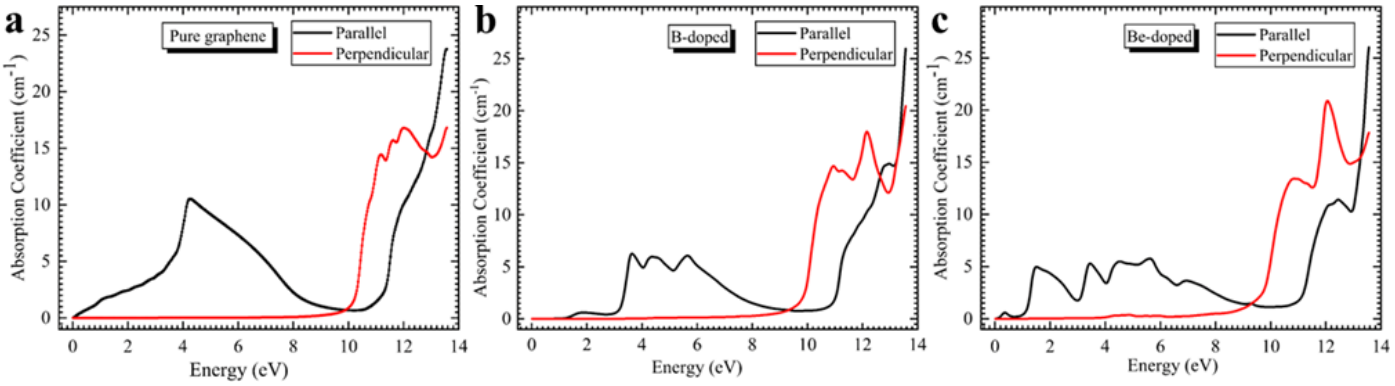

Figure 7. The absorption coefficient of (a) pure graphene (b) B-G (c) Be-G in $E_{\parallel}$ and $E_{\perp}$ polarization.

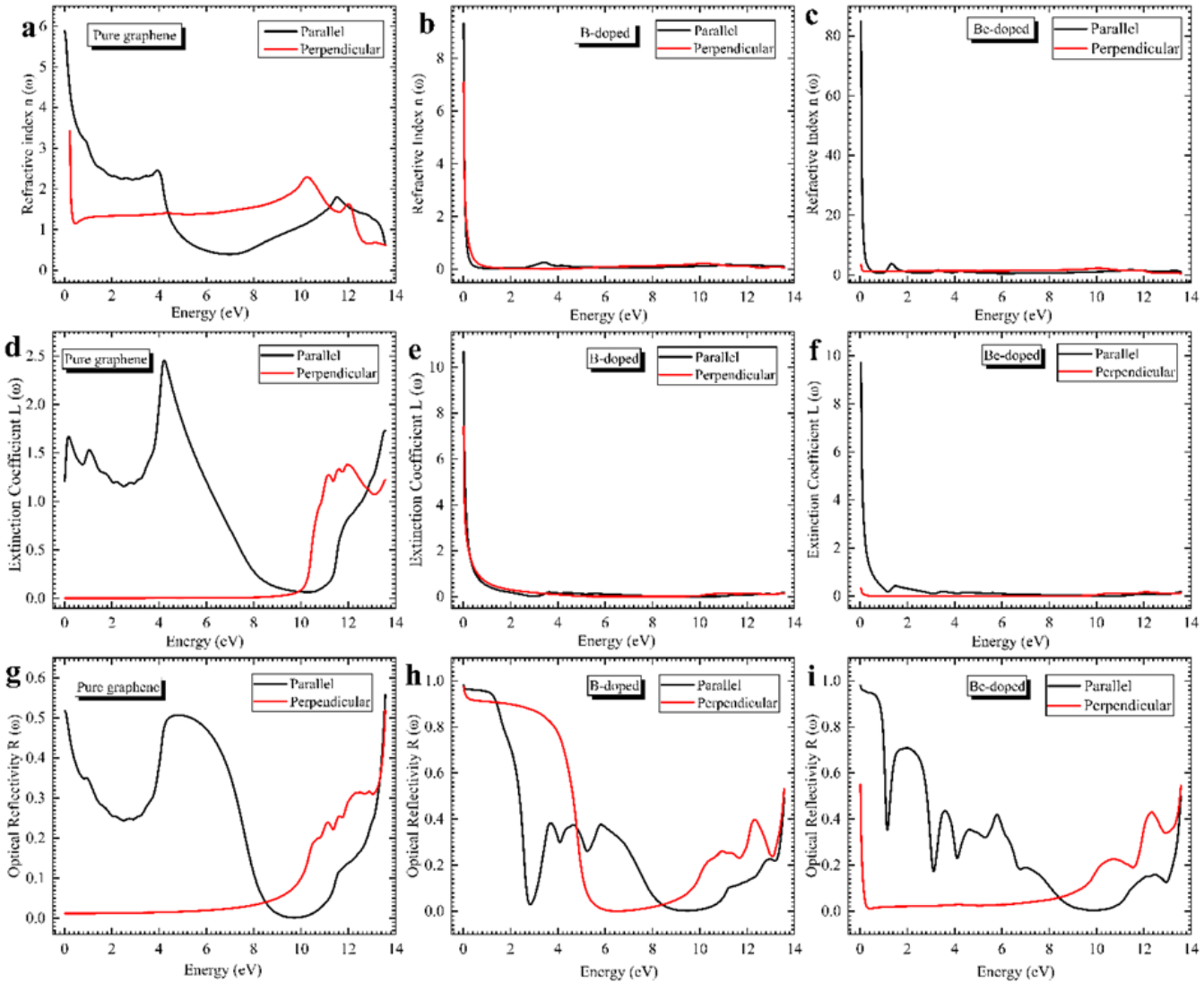

Figure 8. The calculated refractive index of (a) pure (b) B-G and (c) Be-G and the extinction coefficient of (d) pure graphene (e) B (f) Be-G and the reflectivity of (g) of pure graphene (h) B-G (i) Be-G, all in the $E_{\parallel}$ and $E_{\perp}$ polarization.

95 and 3 for the $E_{\parallel}$ and $E_{\perp}$ polarizations, respectively.

Figure 8d-f illustrates the extinction coefficient of the pure graphene and doped systems, and the expression below connects the extinction coefficient with the absorption coefficient

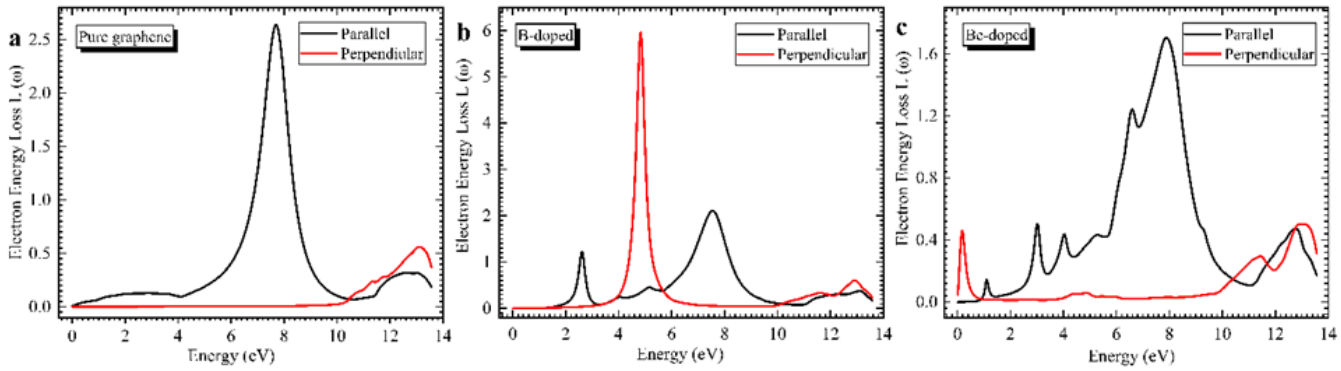

Figure 9. The calculated electron energy loss of (a) pure graphene (b) B-G (c) Be-G, all in the $E_{\parallel}$ and $E_{\perp}$ polarization of light.

[121].

$$A_{coeff}(\omega) = \frac{4\pi K(\omega)}{\lambda}, \tag{10}$$

where the absorption coefficient and light wavelength denoted by A_{coeff} and λ respectively.

The peak obtained at k (ω) of pure graphene in Figure 8d is like the plot's trends seen in the imaginary part of the dielectric function at low energies 0-4eV in the $E_{\parallel}$ polarization of light. Likewise, a similar trend appears in Figure 8e-f when compared with the imaginary absorption coefficient of the doped systems. For pure graphene, a similar increase in the extinction coefficient emerges due to quantum confinement, which falls after reaching its highest value. In Figure 8d. we observed a fall in the extinction coefficient k (ω) at the high energy range in the UV range and a rise again in the infrared region [74]. These fluctuations observed in K (ω) are attributed to the photoelectron effect, the Compton effect, and several other phenomena [75].

In Figure 8g-f, the reflectivity R (ω) of pure, B and Be-G in the $E_{\parallel}$ and $E_{\perp}$ polarization as a function of energy and wavelength emerges. In the $E_{\parallel}$ polarization, pristine graphene's reflectivity intensity reached 0.5 at 4.4 eV in the ultraviolet range. The position of the peak agrees with reports by Olaniyan *et al.* [34] and M. Houmad *et al.* [40]. However, the reflectivity spectrum of pristine graphene in the $E_{\parallel}$ polarization revealed an eigenvalue of 0.24 in the visible region of the electromagnetic spectrum with a value of zero in the range of 8.6 -10.0 eV. The maximum reflectivity intensity value in the $E_{\perp}$ polarization appears at 0.32 eV at 13.2 eV. In both directions, the reflectivity below than 8 eV rises as a function of energy with the reflectivity in the $E_{\perp}$ polarization being higher from 8.2 eV to 13.2 eV in the infrared range.

The B-G in Figure 8(h) demonstrates a shift in the positions and intensities compared to pure graphene. An extended peak at 3.6 eV is observed and another appears at 13.2 eV, relative to the initial peak frequency at 4.4 eV. In the $E_{\perp}$ polarization of the electromagnetic wave, two peaks appear at 10.8 eV and 12.2 eV with an intensity of 0.26 and 0.38, respectively. We also observe an identical disappearing reflectivity highlighted in pure graphene at 8.6 -10.0 eV in B-G in the $E_{\perp}$ polarization. In Figure 8i, the reflectivity of Be-G illustrates its intensities and position, relative to the pure and B-doped graphene $E_{\parallel}$ and $E_{\perp}$ polarization of light.

This system has four peaks in the $E_{\parallel}$ polarization of light at 2.2, 3.8, 6.0, and 12.8 eV, with intensities of 0.7, 0.45, 0.43, and 0.16, respectively. In comparison to the peak at 4.4 eV in pristine graphene, these peaks here show distinct spikes within this range. Notably, peaks at 10.6 eV and 12.2 eV with intensities of 0.23 and 0.43, respectively, are observed in the, polarization. Moreover, all systems considered (pristine, B-doped, and Be-doped graphene) in the polarization fall to zero within the frequency range of 8.6 to 10.2 eV. This suggests a transparent system during this range of frequencies, which corresponds to the ultraviolet range of the EM spectra. These agree with existing studies [34, 76, 77]. The reflectivity in the $E_{\perp}$ polarization of Be-doped graphene from 8.6 eV to 13.2 eV is higher than the $E_{\parallel}$ polarization of light. In the visible range, the reflectivity of Be-G is much less than that of B and pristine graphene, in that order, as illustrated in Figure 8g-i.

3.3.4. Electron Energy Loss of the systems

Electron loss determines the energy distribution of electrons that have interacted with materials and lost energy due to inelastic scattering [77, 78]. Figure 9a-c presents the profile of energy loss functions of pure graphene and the impact of B and Be doped systems on the plasmon oscillations in the $E_{\parallel}$ and $E_{\perp}$ polarizations of graphene. In Figure 9a, two peaks with intensities of 2.7 and 0.4 in the $E_{\parallel}$ polarization appear at 7.8 eV and 13.2 eV. These peaks observed are caused by the excitation of the π and $\pi + \sigma$ plasmons in the $E_{\parallel}$ polarization of electromagnetic waves [67]. In the $E_{\perp}$ polarization, a peak with a height of 0.52 appeared at 13 eV, respectively. The plasmon peaks in the $E_{\perp}$ polarization of light is caused by transitions between occupied and unoccupied states. As shown in Figure 9a, the energy loss function in both $E_{\parallel}$ and $E_{\perp}$ polarization originates at q $\approx$ 0 eV in the long wavelength limit, which determines the plasmon dispersion [79].

Despite differences in peak locations, our calculations are consistent with previous results reported both theoretically and experimentally where the local field effect was used [79–81]. In Figure 9b-c, the electron energy loss of B and Be-G is illustrated in both $E_{\parallel}$ and $E_{\perp}$ polarizations. Three peaks appeared

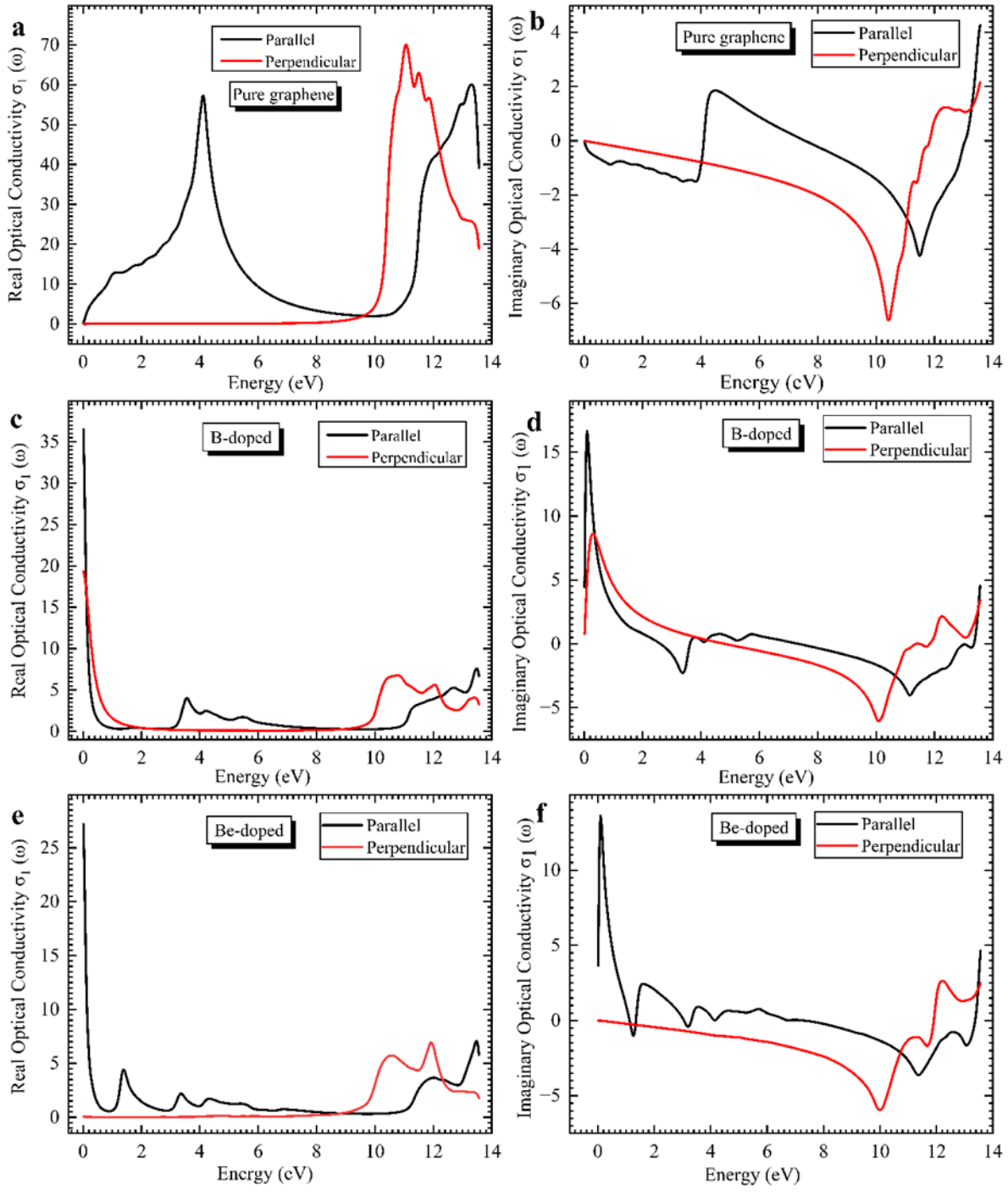

Figure 10. The calculated (a) real optical conductivity of pure graphene (b) imaginary optical conductivity (c) real optical conductivity of B-G (d) imaginary optical conductivity of B (e) real optical conductivity of Be-doped graphene (f) imaginary optical conductivity of Be-doped graphene.

in the direction of B-doped graphene, with the peak at 7.8 eV having the highest intensity at 2.1 eV and the others at 2.3 eV and 13.2 eV with intensities of 1.3 and 0.3, respectively.

Figure 9b illustrates that in the $E_{\perp}$ polarization, a very sharp peak appears at 4.7 eV with an intensity of 5.9 and a less intense peak at 13 eV with a height of 0.6. However, in the $E_{\perp}$ polarization, the introduction of B impurities has modified the position of the q orientations to approximately 1.6 eV. In Figure 9c, the most intense peak in the $E_{\parallel}$ polarization for Be-G appears at 8.1 eV at an intensity of 1.76, with four other peaks at 1.2, 3.2, 4.0, and 13.2 with intensities of 0.12, 0.52, 0.44, and 0.52, respectively. In the $E_{\perp}$ electromagnetic polarization,

three peaks emerge at 0.2 eV, 11.4 eV, and 13.2 eV at 0.4, 0.32, and 0.56. However, the q orientation appears in both the $E_{\parallel}$ and $E_{\perp}$ polarizations at 0.2 and 0.0, respectively.

3.3.5. *Optical Conductivity of the system*

It is a vital parameter in determining the electronic state of materials[130]. The expression relates the refractive index n (ω) with the absorption A (ω):

$$\sigma(\omega) = \frac{A(\omega)\, n(\omega) v}{4\pi} \tag{11}$$

Figure 10a-b illustrates that both the real and imaginary optical conductivity of pristine graphene originates at 0 eV in the $E_{\parallel}$ and $E_{\perp}$ polarization of light due to its gapless property. In Figure 10a, two peaks appear at frequencies of 4.2 eV and 13.6 eV with intensities of 5.3 and 5.4 in the parallel polarization at the UV zone and spread across the visible light range. The peaks are like the peaks observed in pure graphene at the parallel polarization of light of $\varepsilon_1(\omega)$. In the perpendicular polarization of the EM wave, an extended peak appears at 11.4 eV with a height of 6.3. In Figure 10b, for the imaginary conductivity in both the parallel and perpendicular polarization of light, a peak appears in both directions at 4.2 and 12.2 eV with intensities of 2.0 and 1.8, respectively.

The effect of B on the optical conductivity of graphene in the $E_{\parallel}$ and $E_{\perp}$ polarizations of electromagnetic waves was investigated, as indicated in Figure 10a-c. Two peaks appear at 3.6 eV and 13.2 eV with intensities 3.8 and 4 in the parallel polarization of light in Figure 10c. Similarly, at the perpendicular polarization two peaks appear at 11.2 eV and 12.1 eV with intensities of 6.0 and 5.0. However, at 10.4 eV to 13.2 eV, the peak in the perpendicular polarization became greater than the peak in the parallel polarization. In Figure 10d, at the parallel polarization of the electromagnetic wave, two peaks appear at 5.6 eV and 13.4 eV with intensities of 0.2 and 0.1, respectively. Similarly, in the parallel polarization, two peaks appear at 0.2 eV and 12.2 eV with intensities of 8.4 and 2.5, respectively.

However, from 4.4 eV to 10.6 eV, the $E_{\parallel}$ polarization was greater than the $E_{\perp}$ polarization of the electromagnetic wave. Figure 10e-f depicts the influence of Be on the optical conductivity of graphene. In Figure 10e, four peaks are observed in the parallel polarization for the real-optical conductivity at 1.6 eV, 2.44 eV, 12.2 eV, and 13.2 eV with intensities 4, 2, 3.2, and 7, respectively. However, in the $E_{\perp}$ polarization, two peaks emerge at 10.4 eV and 12.2 eV at 6.0 and 7.2, respectively. Similarly, the $E_{\perp}$ polarization of the electromagnetic wave in Be-graphene is greater than the $E_{\parallel}$ polarization of the EM wave in the B-doped system in the 9.4 – 12.2 eV range.

However, the Be-doped model exhibits a more intense peak compared to B-graphene. Figure 10 (f) shows that the imaginary optical conductivity reveals four at 0.2 eV, 1.8 eV, 3.6 eV, and 12.6 with intensities of 13.6, 2.2, 1.6, and below zero in the parallel polarization of light. In the $E_{\perp}$ polarization, two peaks appear at 11.4 eV and 12. 2 eV with intensities below zero and 2.2. However, in the $E_{\perp}$ polarization at 10 eV, the optical reflectivity overlaps at the energy band, and from 10.2 eV to 13.2 eV in this direction, it was greater than the parallel polarization of light. However, B and Be-G were found to be more stable and reduced the conductivity of graphene in the visible light range. The value of the conductivity of Be-doped graphene is 1.2 eV, that of B-doped graphene is 0.2 and that of pristine graphene appears at 0 eV.

4. Conclusion

This study employs density functional theory to investigate the electronic and optical properties of B and Be-doped graphene. The study considered a 2x2x1 graphene supercell with 12.5% substitution of both B and Be, resulting in a band gap of 0.4 and 0.9 eV, respectively. B-doped graphene displays a negligible magnetic moment of -0.00742 μ_B suggesting its potential suitability for catalytic semiconductor devices.

Furthermore, the study demonstrates that in both parallel and perpendicular polarizations, pure graphene as well as B and Be-G exhibit transparency in the frequency range of 8.6 eV to 10.2 eV in the parallel polarization of the electromagnetic spectrum.

This study also demonstrates that the optical conductivity of graphene can be modified with B and Be dopant atoms while preserving the optical transparency of graphene. Overall, these intriguing findings suggest that the band gap of graphene can be tailored for different optoelectronic devices through chemical doping of the system geometry.

Acknowledgement

L. O. Agbolade acknowledges Malaysian International Scholarship (MIS) for funding his Master of Science (M.Sc.) in Nanomaterial Engineering at the Institute of Nano Electronic Engineering, Universiti Malaysia Perlis, MALAYSIA.

References

[1] E. B. Yutomo, F. A. Noor, & T. Winata, "Effect of the number of nitrogen dopants on the electronic and magnetic properties of graphitic and pyridinic N-doped graphene-a density-functional study", RSC Advances **11** (2021) 18371. https://doi.org/10.1039/D1RA01095F.

[2] Y. Zhang, B. Huang, Q. Dong, X. Zhang, C. Chen, J. Yun, Z. Zhang & H. Guo, "Two-dimensional hydrogenated/fluorinated graphyne/graphyne-like BN van der Waals heterostructures and their potential application in ultraviolet photodetection: A theoretical prediction", Applied Surface Science **611** (2023) 155739. https://doi.org/10.1016/j.apsusc.2022.155739.

[3] S. Kumar, S. Kumar, R. N. Rai, Y. Lee, T. H. C. Nguyen, S. Y. Kim, Q. V. Le & L. Singh, "Recent development in two-dimensional material-based advanced photoanodes for high-performance dye-sensitized solar cells", Solar Energy **249** (2023) 606. https://doi.org/10.1016/j.solener.2022.12.013.

[4] J. H Gosling, S. V. Morozov, E. E Vdovin, M. T. Greenaway, Y. N. Khanin, Z. Kudrynskyi, A. Patanè, L. Eaves, L. Turyanska, T. M. Fromhold & O. Makarovsky, "Graphene FETs with high and low mobilities have universal temperature-dependent properties", Nanotechnology **34** (2023) 125702. https://doi.org/10.1088/1361-6528/aca981.

[5] T. A. Oliveira, P. V. Silva, V. Meunier & E. C. Girão, "Tuning the carrier mobility and electronic structure of graphene nanoribbons using Stone–Wales defects", Carbon **201** (2023) 222. https://doi.org/10.1016/j.carbon.2022.08.079.

[6] C. H. Huang, C. H. Wu, R. G. Bikbaev, M. J. Ye, C. W. Chen, T. J. Wang, I. V. Timofeev, W. Lee & K. P. Chen,"Wavelength-and Angle-Selective Photodetectors Enabled by Graphene Hot Electrons with Tamm Plasmon Polaritons", Nanomaterials 1 **13** (2023) 693. https://doi.org/10.3390/nano13040693.

[7] H. Habib, M. Alam, M. Aggarwal, I. S. Wani & S. Husain, "Latest Fabrication Approaches for Surface Modified Carbon Materials: Carbon Nanotubes and Graphene", in *Surface Modified Carbon Nanotubes*, Volume 1: Fundamentals, Synthesis and Recent Trends, American Chemical Society, Washington, 2022, pp. 27-47. https://doi.org/10.1021/bk-2022-1424.ch002.

[8] Huaizhou Jin, Jing-Yu Wang, Xia-Guang Zhang, Weiyi Lin, Weiwei Cai, Yue-Jiao Zhang, Zhi-Lin Yang, Fan-Li Zhang & Jian-Feng Li "Electron transition manipulation under graphene-mediated plasmonic engineering nanostructure", Nano Research **16** (2022) 5376. https://doi.org/10.1007/s12274-022-5209-2.

[9] M. D. Bhatt, H. Kim, & G. Kim, "Various defects in graphene: a review", RSC Advances **12** (2022) 21520. http://dx.doi.org/10.1039/D2RA01436J.

[10] J. Sengupta, C. M. Hussain, "Graphene-Induced Performance Enhancement of Batteries, Touch Screens, Transparent Memory, and Integrated Circuits: A Critical Review on a Decade of Developments", Nanomaterials **12** (2022) 3146. https://doi.org/10.3390/nano12183146

[11] M. Saeed, P. Palacios, M. D. Wei, E. Baskent, C. Y. Fan, B. Uzlu, K. T. Wang, A. Hemmetter, Z. Wang, D. Neumaier, M. C. Lemme, & R. Negra, "Graphene-Based Microwave Circuits: A Review", Advanced Materials **34** (2022) 2108473. https://doi.org/10.1002/adma.202108473.

[12] P. C. Sherrell, M. Fronzi, N. A. Shepelin, A. Corletto, D. A. Winkler, M. Ford, J. G. Shapter & A. V. Ellis, "A bright future for engineering piezoelectric 2D crystals", Chemical Society Reviews **51** (2022) 650. https://doi.org/10.1039/D1CS00844G.

[13] K. T. Santosh , P. Raunak, W. Nannan , K. Vijay , J. S. Olusegun , B. Michał , Z. Yanqiu & K. M. Yogendra, "Progress in Diamanes and Diamanoids Nanosystems for Emerging Technologies", Advanced Science **9** (2022) 2105770. https://doi.org/10.1002/advs.202105770.

[14] V. Sharma, B. Roondhe, S. Saxena & A. Shukla, "Role of functionalized graphene quantum dots in hydrogen evolution reaction: A density functional theory study", International Journal of Hydrogen Energy, **47** (2022) 41748. https://doi.org/10.1016/j.ijhydene.2022.02.161.

[15] E. B. Yutomo, F. A. Noor & T. Winata, "Effect of the number of nitrogen dopants on the electronic and magnetic properties of graphitic and pyridinic N-doped graphene-a density-functional study", RSC Advances **11** (2021) 18371. https://doi.org/10.1039/D1RA01095F.

[16] C. Tian, W. Miao, L. Zhao & J. Wang, "Graphene nanoribbons: Current status and challenges as quasi-one-dimensional nanomaterials", Reviews in Physics **10** (2023) 100082. https://doi.org/10.1016/j.revip.2023.100082

[17] N. Sohal, B. Maity, & S. Basu, "Recent advances in heteroatom-doped graphene quantum dots for sensing applications", RSC Advances **11** (2021) 25586. https://doi.org/10.1039/d1ra04248c

[18] P. Błoń´ski, J. Tucek, Z. Sofer, V. Mazanek, M. Petr, M. Pumera, & R. Zboril, "Doping with Graphitic Nitrogen Triggers Ferromagnetism in Graphene", Journal of the American Chemical Society **139** (2017) 3171. https://doi.org/10.1021/jacs.6b12934

[19] Y. P. Lin, Y. Ksari, J. Prakash, L. Giovanelli, J. C. Valmalette & J. M. Themlin, "Nitrogen-doping processes of graphene by a versatile plasma-based method", Carbon **73** (2014) 216. https://www.sciencedirect.com/science/article/abs/pii/S0008622314001985.

[20] S. Yu, B. Guo, T. Zeng, H. Qu, J. Yang, & J. Bai, "Graphene-based lithium-ion battery anode materials manufactured by mechanochemical ball milling process: A review and perspective", Composites Part B: Engineering, **246** (2022) 110232. https://doi.org/10.1016/j.compositesb.2022.110232.

[21] X. Zhou, C. Zhao, G. Wu, J. Chen, & Y. Li, "DFT study on the electronic structure and optical properties of N, Al, and N-Al doped graphene", Applied Surface Science **459** (2018) 354 https://doi.org/10.1016/j.apsusc.2018.08.015

[22] Q. Luo, S. Yin, X. Sun, Y. Tang, Z. Feng, & X. Dai, "Density functional theory study on the electronic, optical and adsorption properties of Ti-, Fe- and Ni- doped graphene", Diam Relat Mater **128** (2022) 109290. https://doi.org/10.1016/j.diamond.2022.109290.

[23] Y. Fujimoto, "Formation, Energetics, and Electronic Properties of Graphene Monolayer and Bilayer Doped with Heteroatoms", Advances in Condensed Matter Physics **2015** (2015) 571490. https://doi.org/10.1155/2015/571490

[24] S. Ullah, P. A. Denis, & F. Sato, "Beryllium doped graphene as an efficient anode material for lithium-ion batteries with significantly huge capacity: A DFT study", Applied Material Today **9** (2017) 333. https://doi.org/10.1016/J.APMT.2017.08.013

[25] O. Olaniyan & H. Pretoria, *Ab initio study of the beryllium-sulphur and beryllium-nitrogen co-doped graphene for nanoelectronic and optoelectronic devices*. Thesis , University of Pretoria, 2018. http://hdl.handle.net/2263/70465.

[26] M. Yan, Z. Guo, Q. Li, Z. Dai, A. Yu, & C. Sun, "Density Functional Theory Studies on Boron-Modified Graphene Edges for Electroreduction of Nitrogen", ACS Applied Nano Materials **5** (2022) 11270. https://doi.org/10.1021/acsanm.2c02399.

[27] Y. Yamada, H. Tanaka, S. Kubo, & S. Sato, "Unveiling bonding states and roles of edges in nitrogen-doped graphene nanoribbon by X-ray photoelectron spectroscopy", Carbon **185** (2021) 342. https://doi.org/10.1016/j.carbon.2021.08.085.

[28] J. S. David, *Characterization and Evaluation of Materials, Optical and Electronic Materials, Metallic Materials, Pseudopotentials and the LAPW Method Second Edition*, Springer, New York, NY. https://doi.org/10.1007/978-1-4757-2312-0.

[29] P. Blaha, K. Schwarz, F. Tran, R. Laskowski, G. K. H. Madsen, & L. D. Marks, "WIEN2k: An APW+lo program for calculating the properties of solids", Journal of Chemical Physics **152** (2020) 074101. https://doi.org/10.1063/1.5143061.

[30] M. Ernzerhof & G. E. Scuseria, "Assessment of the Perdew-Burke-Ernzerhof exchange-correlation functional", Journal of Chemical Physics **110** (1999) 5029. https://doi.org/10.1063/1.478401.

[31] J. P. Perdew, K. Burke, & Y. Wang, "Generalized gradient approximation for the exchange-correlation hole of a many-electron system", Physical Review B **54** (1996) 16533. https://doi.org/10.1103/PhysRevB.54.16533.

[32] A. A. Adewale, , A. Chik, T. Adam, T. M. Joshua, & M. O. Durowoju, "Optoelectronic behavior of ZnS compound and its alloy: A first principle approach", Materials Today Communications **27** (2021) 102077. https://doi.org/10.1016/j.mtcomm.2021.102077

[33] H. J. Monkhorst & J. D. Pack, "Special points for Brillonin-zone integrations" **13** (1976) 5188. https://doi.org/10.1103/PhysRevB.13.5188

[34] O. Olaniyan, R. E. Maphasha, M. J. Madito, A. A. Khaleed, E. Igumbor, & N. Manyala, "A systematic study of the stability, electronic and optical properties of beryllium and nitrogen co-doped graphene", Carbon **129** (2018) 207. https://doi.org/10.1016/j.carbon.2017.12.014

[35] B. Bhattachary & U. Sarkar, "The Effect of Boron and Nitrogen Doping in Electronic, Magnetic, and Optical Properties of Graphyne", The Journal of Physical Chemistry *C* **120** (2016) 26793. https://doi.org/10.1021/acs.jpcc.6b07478.

[36] C. Ambrosch-Draxl & J. O. Sofo, "Linear optical properties of solids within the full-potential linearized augmented planewave method", Computer Physics Communications **175** (2006) 1. https://doi.org/10.1016/j.cpc.2006.03.005.

[37] V. V. Tuan , D. P. Khang , N. P. Tri , D. V. Dat , T. D. Phuc , V. N. Chuong , V. P. Huynh, T. T. B. Nguyen, D. M. Hoatdi & N. H. Nguyen, "First-principles prediction of chemically functionalized In N monolayers: Electronic and optical properties", RSC Advances **10** (2020) 10731. https://doi.org/10.1039/D0RA01025A.

[38] P. Nath, S. Chowdhury, D. Sanyal, & D. Jana, "Ab-initio calculation of electronic and optical properties of nitrogen and boron doped graphene nanosheet", Carbon **73** (2014) 275. https://doi.org/10.1016/j.carbon.2014.02.064.

[39] M. Rizwan, S. Aleena, M. Shakil, T. Mahmood, A. A. Zafar, T. Hussain, & M.H. Farooq,"A computational insight of electronic and optical properties of Cd-doped BaZrO3", Chinese Journal of Physics **66** (2020) 318. https://doi.org/10.1016/j.cjph.2020.04.022

[40] M. Houmad, H. Zaari, A. Benyoussef, A. el Kenz, & H. Ez-Zahraouy, "Optical conductivity enhancement and band gap opening with silicon doped graphene", Carbon **94** (2015) 1021. https://doi.org/10.1016/j.carbon.2015.07.033

[41] R. Sharma, S. Khan, V. Goyal, V. Sharma, & K. S. Sharma, "Investigation on effect of boron and nitrogen substitution on electronic structure of graphene", FlatChem **1** (2017) 20. https://doi.org/10.1016/j.flatc.2016.

10.001
[42] R. Saito, A. Jorio, J. Jiang, K. Sasaki, , G. Dresselhaus, & M. S. Dresselhaus, "Optical properties of carbon nanotubes and nanographene", in *Oxford Handbook of Nanoscience and Technology*, 2010, 1–30. https://doi.org/10.1093/oxfordhb/9780199533053.013.1
[43] T. Wang, N. Zhao, C. Shi, L. Ma, F. He, C. He, J. Li, & E. Liu "Interface and Doping Effects on Li Ion Storage Behavior of Graphene/Li2O",The Journal of Physical Chemistry C **121** (2017) 19559. https://doi.org/10.1021/acs.jpcc.7b04642.
[44] P. Rani & V. K. Jindal, "Designing band gap of graphene by B and N dopant atoms", RSC Advances **3** (2013) 802. https://doi.org/10.1039/c2ra22664b
[45] K. Zhao, W. Zhang5, L. Peng, M. Jiang, W. Wang, X. He, Y. Wang & L. Gao "First-principle study on electronic and optical properties of (Al, P, Al-P) doped graphene", Material Research Express **7** (2020) 105013. https://doi.org/10.1088/2053-1591/abc125.
[46] T. Ando, "The electronic properties of graphene and carbon nanotubes", Npg Asia Materials **1** (2009) 17. https://www.nature.com/articles/am200923.
[47] B. Y. Wang , H. Wang , L. Y. Chen , H. C. Hsueh , X. Li, J. Guo , Y. Luo , J. W. Chiou, W. H. Wang , P.H Wang , K. H. Chen , Y. C. Chen , L. C. Chen , C. H. Chen, J. Wang & W. F. Pong "Nonlinear bandgap opening behavior of BN co-doped graphene", Carbon **107** (2016) 857. https://doi.org/10.1016/J.CARBON.2016.06.091
[48] S. Mukherjee & T. P. Kaloni, "Electronic properties of boron- and nitrogen-doped graphene: A first principles study", Journal of Nanoparticle Research **14** (2012) 1059. https://doi.org/10.1007/s11051-012-1059-2.
[49] B. Bhattacharya & U. Sarkar, "The Effect of Boron and Nitrogen Doping in Electronic, Magnetic, and Optical Properties of Graphyne", The Journal of Physical Chemistry C **120** (2016) 26793. https://doi.org/10.1021/acs.jpcc.6b07478.
[50] S. Ullah, P. A. Denis, & F. Sato, "Beryllium doped graphene as an efficient anode material for lithium-ion batteries with significantly huge capacity: A DFT study", Applied Material Today **9** (2017) 333. https://doi.org/10.1016/J.APMT.2017.08.013
[51] X. S. Dai, T. Shen, & H. C. Liu, "DFT study on electronic and optical properties of graphene modified by phosphorus", Material Research Express **6** (2019) 085635. https://doi.org/10.1088/2053-1591/ab29bc
[52] M. L. Ould NE, A. G. el hachimi, M. Boujnah, A. Benyoussef, & A. el Kenz, "Comparative study of electronic and optical properties of graphene and germanene: DFT study",Optik (Stuttg) **158** (2018) 693. https://doi.org/10.1016/j.ijleo.2017.12.089
[53] Z. M. Wang, , A. Woag & G. Salamo, *Lecture notes in nanoscale science and technology*, Springer book series, 2023. https://www.springer.com/series/7544
[54] H. Ahmad, J. Lindemuth, Z. Engel, C. M. Matthews, T. M. McCrone, & W. A. Doolittle, "Substantial P-Type Conductivity of AlN Achieved via Beryllium Doping", Advanced Materials **33** (2021) 2104497. https://doi.org/10.1002/adma.202104497
[55] A. C. F. Serraon, J. A. D. Del Rosario, P. Y. A. Chuang, M. N. Chong, Y. Morikawa, A. A. B. Padama & J. D. Ocon, "Alkaline earth atom doping-induced changes in the electronic and magnetic properties of graphene: a density functional theory study", RSC Advices **11** (2021) 6268. https://doi.org/10.1039/D0RA08115A.
[56] X. Y. Liang, N. Ding, S. P. Ng, & C. M. L. Wu, "Adsorption of gas molecules on Ga-doped graphene and effect of applied electric field: A DFT study", Applied Surfuce Science, **411** (2017) 11. https://doi.org/10.1016/J.APSUSC.2017.03.178
[57] V. V. Chaban & O. v. Prezhdo, "Boron doping of graphene-pushing the limit", Nanoscale **8** (2016) 15521. https://doi.org/10.1039/c6nr05309b
[58] A. A. Adewale, A. Chik, O. K. Yusuff, S. A. Ayinde & Y. K. Sanusi, "First principle calculation of structural, electronic and optical properties of CdS and doped Cdx-1AxS (A=Co, Fe, Ni) compounds", Material Today Communication **26** (2021) 101882. https://doi.org/10.1016/j.mtcomm.2020.101882.
[59] A. Omidvar, "Electronic structure tuning and band gap opening of nitrogen and boron doped holey graphene flake: The role of single/dual doping", Material Chemistry Physic **202** (2017) 258. https://doi.org/10.1016/J.MATCHEMPHYS.2017.09.025.
[60] F. López-Urías, M. Terrones & H. Terrones, "Beryllium doping graphene, graphene-nanoribbons, C60-fullerene, and carbon nanotubes", Carbon **84** (2015) 317. https://doi.org/10.1016/J.CARBON.2014.11.053.
[61] O. Olaniyan, E. Igumbor, A. A. Khaleed, A. A. Mirghni & N. Manyala, "Ab-initio study of the optical properties of beryllium-sulphur co-doped graphene", AIP Advances **9** (2019) 025221. https://doi.org/10.1063/1.5060708.
[62] X. He, Z.-X. Chen & Z. Li, "Communication: Emergence of localized magnetic moment at adsorbed beryllium dimer on graphene", Journal of Chemical Physics **133** (2010) 231104. https://doi.org/10.1063/1.3524830.
[63] N. Dhar & D. Jana, "Effect of beryllium doping and vacancy in band structure, magnetic and optical properties of free standing germanene", Current Applied Physics **17** (2017) 1589. https://doi.org/10.1016/j.cap.2017.08.022
[64] H. Ferjani, Y. ben Smida, D. C. Onwudiwe, N. Y. Elamin, S. Ezzine & N. S. Almotlaq, "An Experimental and Theoretical Study of the Optical Properties of (C 2 H 7 N 4 O) 2 BiCl 5 for an Optoelectronic Application", Inorganics **10** (2022) 48. https://doi.org/10.3390/inorganics10040048
[65] M. Junaid Iqbal Khan, Zarfishan Kanwal, Masood Yousaf, Azeem Nabi, Javed Ahmad, Abid Latif & Hamid Ullah, "Investigating structural, electronic and optical properties of CdS:Cr (A GGA and GGA+U study", Solid State Sciences **108** (2020) 106437. https://doi.org/10.1016/j.solidstatesciences.2020.106437.
[66] O. V. Sedelnikova, L. G. Bulusheva, & A. V. Okotrub, "Ab initio study of dielectric response of rippled graphene", Journal of Chemical Physics **134** (2011) 24. https://doi.org/10.1063/1.3604818.
[67] X. Dai, T. Shen, Y. Feng, B. Yang, & H. Liu, "DFT investigations on photoelectric properties of graphene modified by metal atoms", Ferroelectrics **568** (2020) 143. https://doi.org/10.1080/00150193.2020.1811038.
[68] R. Santosh & V. Kumar, *Optical properties of hydrogenated graphene using first-principle calculations*, 2018 5th IEEE Uttar Pradesh Section International Conference on Electrical, Electronics and Computer Engineering (UPCON), Gorakhpur, India, (2018) 1-3. https://doi.org/10.1109/UPCON.2018.8596939.
[69] X. S. Dai, T. Shen, Y. Feng, & H. C. Liu, "Structure, electronic and optical properties of Al, Si, P doped penta-graphene: A first-principles study", Physica B Condens Matter **574** (2019) 411660. https://doi.org/10.1016/j.physb.2019.411660.
[70] P. Rani, G. S. Dubey, & V. K. Jindal, "DFT study of optical properties of pure and doped graphene", Physica E: Low-dimensional Systems and Nanostructures **62** (2014) 28. https://doi.org/10.1016/j.physe.2014.04.010.
[71] S. Hussain, , G. Murtaza, S. H. Khan, A. Khan, M. A. Ali, M. Faizan, A. Mahmood & R. Khenata, "First principles study of structural, optoelectronic and thermoelectric properties of Cu2CdSnX4 (X = S, Se, Te) chalcogenides", Material Research Bulletin **79** (2016) 73. https://doi.org/10.1016/j.materresbull.2016.03.001.
[72] S. Hussain, L. Guo, H. Louis, S. Zhu & T. He, "First-principles calculations of wurtzite ZnS1-xSex solid solutions for photocatalysis", Material Today Communication **21**(2019) 100672. https://doi.org/10.1016/j.mtcomm.2019.100672
[73] M. J. Iqbal Khan & Z. Kanwal, "Investigation of optical properties of CdS for various Na concentrations for nonlinear optical applications (A DFT study)", Optik **193** (2019) 16298. https://doi.org/10.1016/j.ijleo.2019.162985
[74] M. A. Lahiji & A. A. Ziabari, "First–principle calculation of the elastic, band structure, electronic states, and optical properties of Cu–doped ZnS nanolayers", Physica B: Condensed Matter **501** 146. https://doi.org/10.1016/j.physb.2016.08.033.
[75] O. Olaniyan, E. Igumbor, A. A. Khaleed, A. A. Mirghni, & N. Manyala, "Ab-initio study of the optical properties of beryllium-sulphur co-doped graphene, AIP Advances **9** (2019) 025221. https://doi.org/10.1063/1.5060708.
[76] P. Rani, G. S. Dubey & V. K. Jindal, "DFT study of optical properties of pure and doped graphene", Physica E: Low-dimensional systems and nanostructures **62** (2014) 28. https://doi.org/10.1016/J.PHYSE.2014.04.010
[77] R. F. Egerton, "Electron energy-loss spectroscopy in the TEM", Reports on Progress in Physics **72** (2009) 016502. https://doi.org/10.1088/0034-4885/72/1/016502
[78] T. Stauber & G. Gómez-Santos, "Plasmons in layered structures including graphene", New Journal of Physics **14** (2012) 105018. https://doi.org/10.

1088/1367-2630/14/10/105018.

[79] T. Eberlein, U. Bangert, R. R. Nair, R. Jones, M. Gass, A. L. Bleloch, K. S. Novoselov, A. Geim, & P. R. Briddon "Plasmon spectroscopy of free-standing graphene films", Physical Review B: Condensed Matter and Materials Physics **77** 2008. https://doi.org/10.1103/PhysRevB.77.233406

[80] P. Nath, S. Chowdhury, D. Sanyal, & D. Jana, "Ab-initio calculation of electronic and optical properties of nitrogen and boron doped graphene nanosheet", Carbon **73** (2014) 275. https://doi.org/10.1016/j.carbon.2014.02.064.

[81] M. A. Lahiji & A. A. Ziabari, "First–principle calculation of the elastic, band structure, electronic states, and optical properties of Cu–doped ZnS nanolayers", Physica B: Condensed Matter **501** (2016) 146. https://doi.org/10.1016/j.physb.2016.08.033.